

SiO₂-g-Polyisoprene Particle Brush Reinforced Advanced **Elastomer Nanocomposites Prepared via ARGET ATRP**

Yingxue Liu, Zongyu Wang, Yugi Zhao, Guanyi Hou, Ruifeng Jiang, Michael R. Bockstaller, Xuan Qin,* Liqun Zhang,* and Krzysztof Matyjaszewski*

Nanoparticle reinforcement is a general approach toward the strengthening of elastomer nanocomposite in large-scale applications. Extensive studies and efforts have been contributed to demonstrating the property reinforcement of polymer nanocomposites in relation to matrix-filler and filler-filler interaction. Here, a facile synthetic method is creatively reported to synthesize SiO_{2.15/120}-g-polyisoprene (SiO₂-g-PI) particle brushes using atom transfer radical polymerization (ATRP). The dispersion and microstructures of the nanoparticles in the nanocomposites are investigated by morphological characterizations, whereas the reinforcing mechanism is studied through mechanical measurements as well as computational simulation. Remarkably, compared with the cured bulk elastomers and matrix(M)/SiO₂ blends, M/particle brushes (PB) exhibit significant improvement in mechanical properties, including tensile strength, elongation at break, modules, and rolling resistance. This elastomer nanocomposites afford a novel prospect for the practical application of next-generation automobile tires with enhanced performance.

Y. Liu, X. Qin, L. Zhang State Key Laboratory of Organic-Inorganic Composites Beijing University of Chemical Technology Beijing 100029, China

E-mail: qinxuan@mail.buct.edu.cn; zhanglq@mail.buct.edu.cn

Z. Wang, X. Qin, K. Matyjaszewski Department of Chemistry Carnegie Mellon University 4400 Fifth Avenue, Pittsburgh, PA 15213, USA

E-mail: matyjaszewski@cmu.edu

Y. Zhao, M. R. Bockstaller

Department of Materials Science & Engineering Carnegie Mellon University 5000 Forbes Avenue, Pittsburgh, PA 15213, USA

College of Chemistry and Materials Engineering Beijing Technology and Business University 33th Fucheng Road, Beijing 100048, China

R. Jiang Hainan University 58th Renmin Avenue, Haikou, Hainan 570228, China

Institute of Emergent Elastomers School of Materials Science and Engineering South China University of Technology Guangzhou, Guangdong 510640, China

The ORCID identification number(s) for the author(s) of this article can be found under https://doi.org/10.1002/adfm.202315741

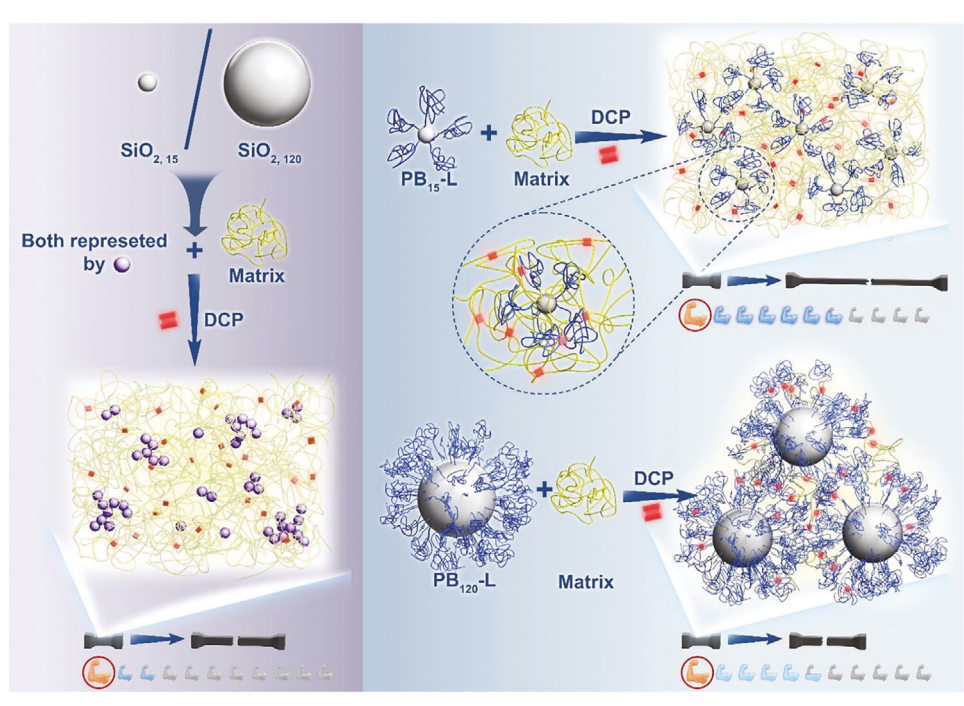
DOI: 10.1002/adfm.202315741

1. Introduction

Polymers implanted with nanofillers, recognized as polymer nanocomposites, have been extensively dedicated to appealing materials in automotive, [1,2] packaging, optics, and capacitors^[3] applications, due to their capability to enhance the physical performance of the pristine polymeric matrices.[4-7] Among different polymer nanocomposites, elastomers reinforced with nanoparticles are strategically valuable and indispensable to a large variety of high-tech and practical applications,[8] most importantly in enhancing the energy efficiency of tire applications.[9-11] In order to achieve the goal of reducing energy consumption by 20%, the European Union promulgated tire labeling mandatory on November 1, 2012. The transportation sector accounts for ≈20% of global energy consumption. Therefore, reducing the

rolling resistance of tires is an important means to reduce energy consumption in the field of transportation.[12] It is well known that embedding nanofillers in neat polymers can effectively reinforce their properties, including mechanical, optical, and thermal properties.[13-15] Nevertheless, in most cases the blends of hydrophobic polymers and hydrophilic nanofillers are prone to be immiscible, making it difficult to control their spatial dispersion.^[16] This spatial organization is mainly due to the strong van der Waals interactions among the nanofillers as well as the entropic depletion attraction. [17-20] Previously, several approaches have been proposed to address this dilemma in the context of elastomers, such as using surfactants, coating/coupling agents, and functional polymeric ligands.[21-24] However, these in situ approaches are greatly limited by the reaction kinetics of reagent molecules and functional chains attached to the nanofiller surfaces.^[25] On the other hand, pre-grafting polymers onto the nanoparticles aids in facilitating and improving dispersibility using variations including the ligand chain length and graft density.[26-29] These parameters leverage the surface characteristics of hydrophilic nanoparticles boned with hydrophobic ligands to further assemble into various macroscopic superstructures. Grafted polymer ligands on the nanoparticle surface can afford sufficient steric stabilization, preventing filler agglomeration, in contrast, the tail-like conformation of homopolymers can bridge the adjacent nanoparticles, hampering the dispersion of nanoparticles.[30-34]

witey.com/doi/10.1002/adfm.202315741 by Carnegie Mellon University. Wiley Online Library on [30.01/2025]. See the Terms and Conditions (https://onlinelibrary.wiley.com/terms-and-conditions) on Wiley Online Library for rules of use; OA acries are governed by the applicable Creative Commons



Scheme 1. Preparation of PI/SiO₂ nanocomposites.

In this contribution, linear polyisoprene (PI) and SiO_{2,15/120}-g-PI particle brushes with high molar mass were prepared through activators regenerated by electron transfer (ARGET) atom transfer radical polymerization (ATRP), Scheme S1 (Supporting Information).^[35–38] The surface modification of nanoparticles with the grafted polymer ligands serves the purpose of exploiting a favorable interaction between the nanoparticles and the polymeric matrix. The cured rubber nanocomposites were obtained for studies focused on understanding the impact of different dispersion states, particle sizes, and polymer chain lengths on mechanical properties. Accordingly, a considerable number of experiments and simulation studies have been committed to revealing the relations between interfacial polymers, microstructures, and macroscopic properties of polymer nanocomposites.

2. Results and Discussion

Controlled radical polymerization enables control over molecular weight and dispersity and has been broadly employed in the synthesis of complex macromolecular structures^[39] with a broad selection of monomers.^[40] Although, the industrial manufacturing of polymers based on low boiling point conjugated 1,3dienes (butadiene, bp = -4.4 °C; isoprene, bp = 34 °C) ranks in the billions of pounds/year, [41,42] unlike the vast literature for nongaseous monomers (styrene and (meth)acrylates),[43-53] very few papers address the polymerization of dienes (mostly isoprene) through controlled radical polymerizations.[54-60] SiO₂-g-PI particle brushes nanofillers (PB_{15} -S, PB_{15} -L, PB_{120} -L, Table S5, Supporting Information) with 15 and 120 nm SiO₂ nanoparticles were synthesized through activator regenerated by electron transfer surface-initiated atom transfer radical polymerization (ARGET SI-ATRP), and linear PI homopolymer (L-1, $M_{\rm n}$ = 204000) was prepared as the polymeric matrix. The benefit of ARGET ATRP is that the amount of copper catalyst in the reaction can be substantially reduced, as the CuII/L species generated via oxidation/radical termination are rapidly converted to active Cu^I/L complexes by the reducing agent. A low concentration Cu^{II} and highly active ligand Me₆TREN were determined as the catalyst/ligand system. Tuning the targeted molecular weight and monitoring polymerization time enabled the synthesis of particle brushes with high molar mass ($M_n = 97\,000/308\,000/37\,9000$, Figures S1 and S2, Supporting Information) and different grafting densities ($\sigma = 0.011/0.007/0.161 \text{ chain/nm}^{-2}$). Due to the low apparent grafting density, particle string/cluster structures were expected in the SiO_{2,15}-g-PI particle brushes.^[61-63]The obtained particle brushes were blended into the linear PI matrix (Table \$1, Supporting Information) and cured by dicumyl peroxide (DCP) at 151 °C to prepare three M/PB nanocomposites $(M/PB_{15}-S, MB/PB_{15}-L, M/PB_{120}-L)$ with 30 wt% SiO₂ contents. The M/SiO₂ reference samples with silica but without polymer brushes (M/SiO_{2,15} and M/SiO_{2,120}) were prepared for comparison, Scheme 1.

To study the nanocomposites' morphology, AFM, SEM, and TEM were employed to evaluate the dispersibility of SiO_2 and PB nanofillers in the PI rubber composites. SEM was utilized to scan the brittle surfaces (triggered by liquid nitrogen) of M/SiO_{2,15}, M/SiO_{2,120}, M/PB₁₅-L, M/PB₁₅-S, and M/PB₁₂₀-L composites, the images are shown in **Figure 1**. The agglomerations of SiO_2 nanoparticles are evident in nanocomposites that were fabricated using the pristine SiO_2 nanoparticles, which have a detrimental influence on the properties of the neat PI matrix. In agreement with SEM results, the TEM images of the micro-sectioned films also verify the presence of large agglomerates of nanoparticles in M/SiO_{2,15} and M/SiO_{2,120}, **Figure 2a,g**. The significant improvements in dispersion were observed in Figure **2c,e,i** as well as the particle/cluster size distribution after the introduction of the PI

wiley.com/doi/10.1002/adfm.202315741 by Carnegie Mellon University, Wiley Online Library on [30/01/2025]. See the Terms

on Wiley Online Library for rules of use; OA articles are governed by the applicable Creative Commons

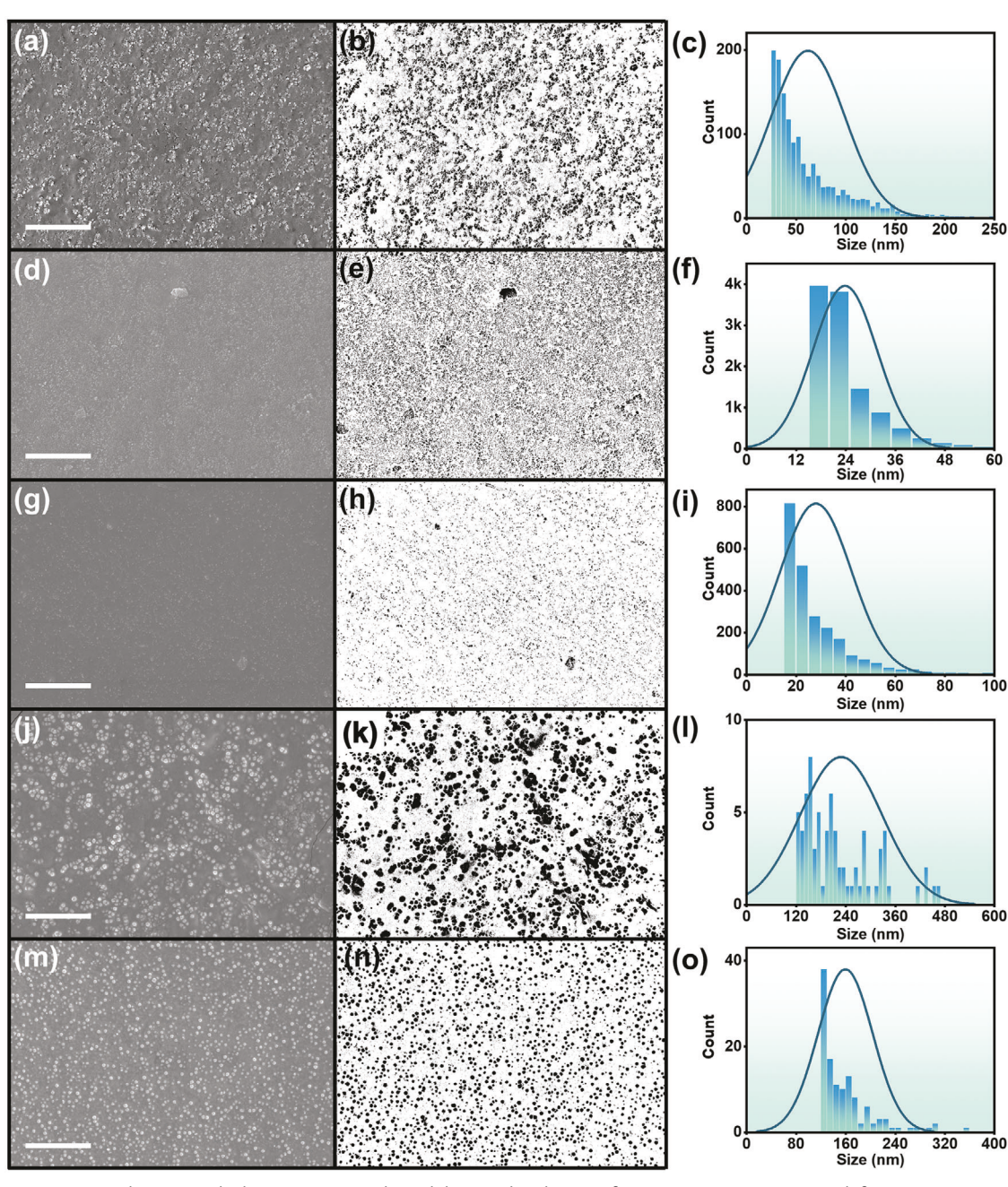


Figure 1. SEM images, analysis (particle domain recognized), and the size distribution of M/SiO_{2,15}: a–c); M/PB₁₅-S: d–f); M/PB₁₅-L: g–i); M/SiO_{2,120}: j–l); M/PB₁₂₀-L: m–o). Scale bars: 2.5 μ m.

ligands on the surface of ${\rm SiO_2}$ nanoparticles. Moreover, due to the low grafting density of the polymer ligands, cluster/string-like structures were seen in M/PB₁₅-S and M/PB₁₅-L, while separated particles were obtained in M/PB₁₂₀-L with high grafting density, Table S5 (Supporting Information).

Elastomeric nanocomposites consist of nanostructured solid fillers and cross-linked polymers. The crosslinking density of the cured elastomer nanocomposites greatly affects their mechanical performance. The solid-state nuclear magnetic resonance (NMR) was used to determine the cross-linking density of the cured nanocomposites. As shown and summarized in

Figure S5 and Tables S6 and S7 (Supporting Information), very close crosslinking density values (27–30%) were obtained among all six specimens.

Strengthening of rubbers by traditionally embedding particulate fillers including precipitated silica or amorphous carbon is of great practical significance in the rubber industry, such as the improvement of the stiffness, modulus, tensile strength, tear strength, and cracking/fatigue/abrasion resistance.^[64] Mechanical property characterizations analyze the reinforcing effect of nanofillers. The stress–strain curves of cured linear PI homopolymer, M/SiO₂, and M/PB nanocomposites are displayed in

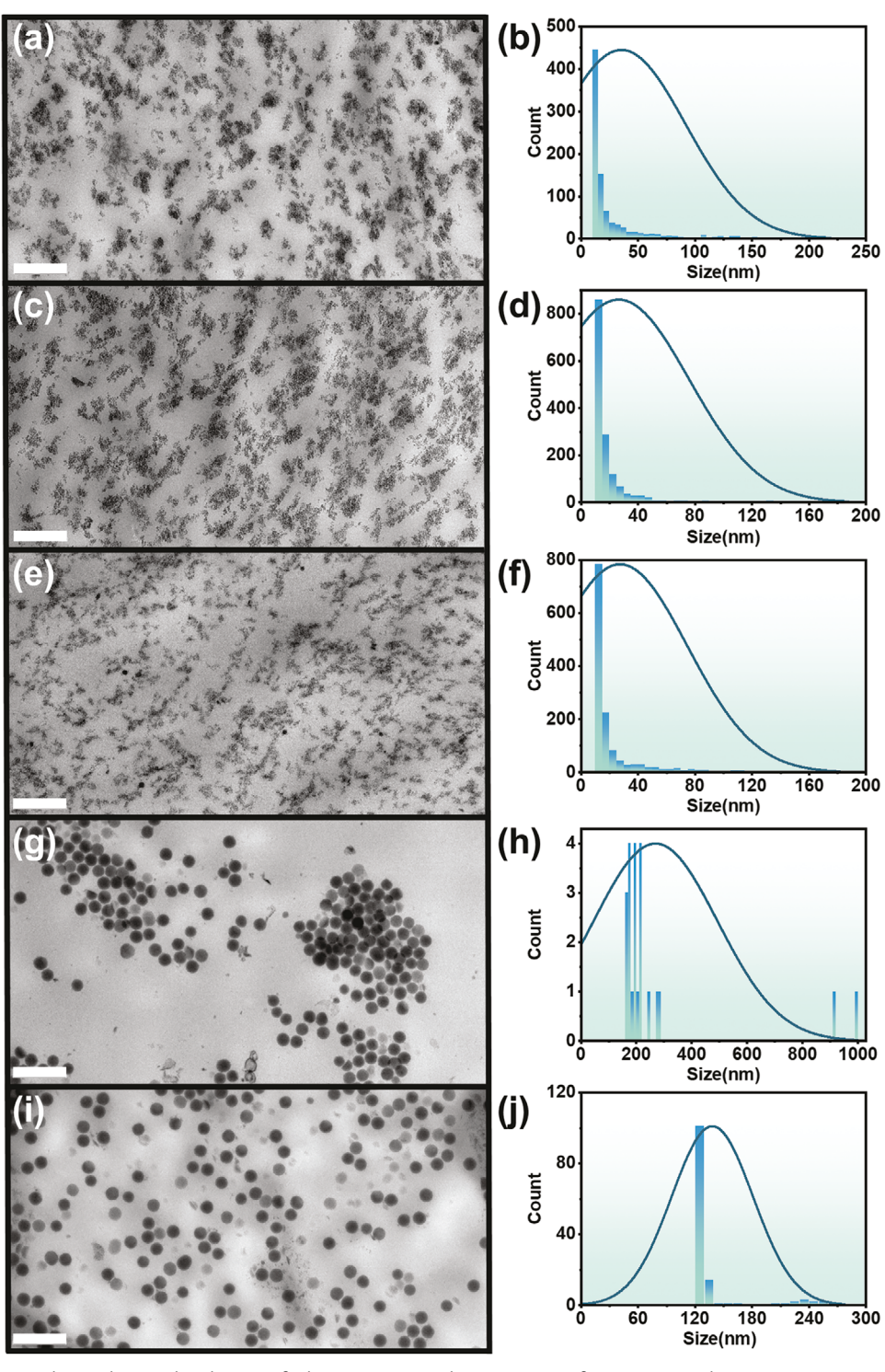


Figure 2. TEM images and particle size distribution of a,b): $M/SiO_{2,15}$, c,d): M/PB_{15} -S, e,f): M/PB_{15} -L, g,h): $M/SiO_{2,120}$, i,j): M/PB_{120} -L, scale bar: 500 nm.

Figure 3a. Tensile strength and elongation at the break of each sample are shown in **Table 1**, Figure 3b. Comparing the cured linear PI with $M/SiO_{2,15}$ and $M/SiO_{2,120}$ nanocomposites, as expected, both tensile strength and elongation at break at a given strain increased with a fixed filler loading (\approx 30 wt%). Besides,

a further performance improvement ($\sigma=1.8 \rightarrow 5.0/5.8$ MPa, $\epsilon=285 \rightarrow 510/680\%$) was observed from M/SiO_{2,15} to M/PB₁₅-S and M/PB₁₅-L, which reveals the superior property reinforcement of the nano-silica fillers and thus the stable covalent bonding between the SiO₂ nanoparticles and the grafted PI ligands.

of use; OA articles are governed by the applicable Creative Commons

16163028, 2024, 26, Downloaded from https://advanced

onlinelibrary.wiley.com/doi/10.1002/adfm.202315741 by Carnegie Mellon University, Wiley Online Library on [3/0/1/2025]. See the Terms and Conditions (https://onlinelibrary.wiley.com/

ms) on Wiley Online Library for rules of use; OA articles are governed by the applicable Creative Commons License

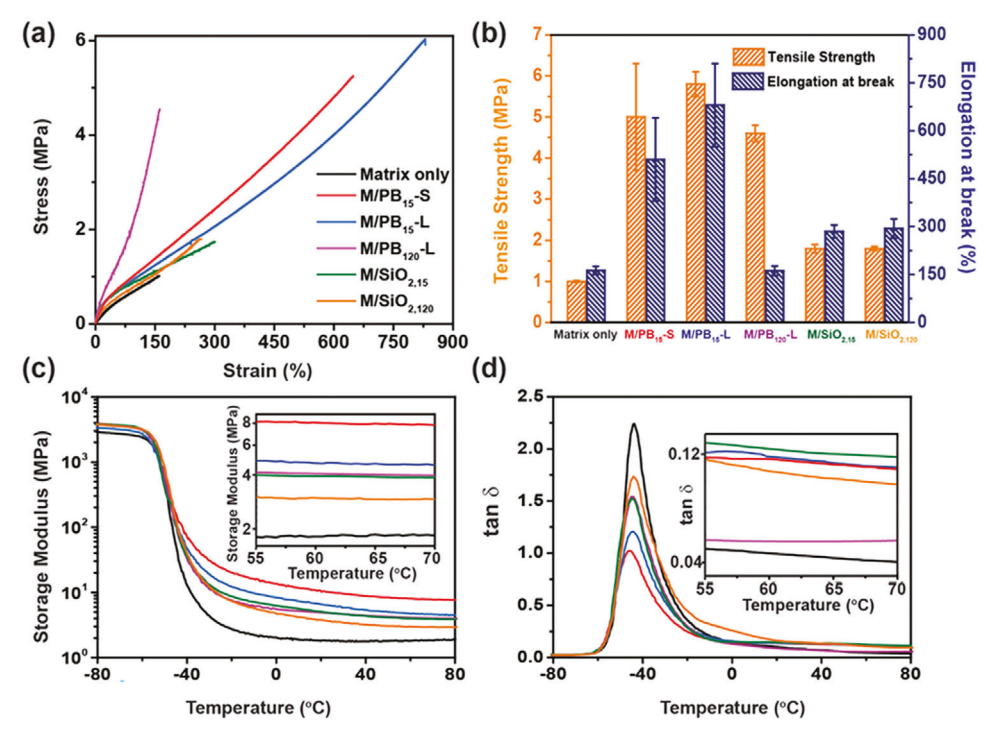


Figure 3. a) Stress—strain curves of cured PI and PI/SiO₂ nanocomposites; b) Plots of the tensile strength and elongation at break of cured PI and PI/SiO₂ nanocomposites; c) Storage modulus G' (inset: G' from 55 to 70 °C); d) loss factor tan δ (inset: tan δ from 55 to 70 °C) for M/SiO₂ and M/PB nanocomposites, black: matrix only, red: M/PB₁₅-S, blue: M/PB₁₅-L, magenta: M/PB₁₂₀-L, olive: M/SiO_{2,15}, orange: M/SiO_{2,120}.

The presence of polymer ligands attached to the nanoparticle surfaces promoted the dispersion and facilitated sufficient chain alignment and orientation among adjacent nanoparticles to greatly enhance the resistance to external stress, leading to an even stress distribution, thereby highly efficient strengthening for the nanocomposites. [8.65–68] On the other hand, the same trend -was also observed in tensile strength between M/SiO_{2,120} and M/PB₁₂₀-L ($\sigma=1.8 \rightarrow 4.6$ MPa). One of the origins of the reinforcing effect in polymer nanocomposite is the introduction of the interfacial polymers surrounding the nanoparticle surface, [69,70] generated via chemical grafting. The interfacial polymers have characteristic structural and dynamic features distinguished from homogenous neat polymers. [71–74] Additionally, the interfacial polymers greatly affect the interactions between nanoparticles, altering nanoparticle microstructures in

nanocomposites, which eventually influences the macroscopic properties of nanocomposites as well. [75] For instance, the elongation at the break value of the M/PB $_{120}$ -L decreased to 162% compared to the value of M/SiO $_{2,120}$, 294%, this stiffening effect can be attributed to the low linear PI loading (3.2 wt%) in the nanocomposites, Table S1 (Supporting Information). Furthermore, comparing cured linear PI and M/SiO $_{2}$ nanocomposites with M/PB nanocomposites, as expected, there is a significant performance improvement in both tear strength and abrasion resistance owing to the presence of grafted PI ligands, Table S8 and Figures S12–S14 (Supporting Information).

The dynamic mechanical analysis (DMA) has particularly high sensitivity and resolution to the physio-chemical cross-linking density, modulus, and viscoelasticity of the cured specimens.^[76] The dynamic mechanical properties of the M/SiO₂ and M/PB

Table 1. Properties of cured PI, M/SiO₂, and M/PB nanocomposites.

Entry	f _{ino} [%] ^{a)}	<i>T</i> _σ [°C] ^{b)}	T, [°C] ^{c)}	E [MPa] ^{d)}	ε [%] ^{d)}	G' [MPa] at 60 °C ^{e)}	tan δ at 60 °C ^{e)}	Hardness
Matrix only	- Jino t- 1			1.0	163	1.81	0.046	46
M/PB ₁₅ -S	33.0	-58.0	-45.9	5.0	510	8.02	0.116	61
M/PB ₁₅ -L	27.4	-56.6	-44.2	5.8	680	4.72	0.119	52
M/PB ₁₂₀ -L	30.5	-57.8	-44.8	4.6	162	4.12	0.056	61
M/SiO _{2,15}	28.6	-56.2	-44.3	1.8	285	4.00	0.124	53
M/SiO _{2,120}	29.6	-57.3	-43.3	1.8	294	2.99	0.107	52

^{a)} The fraction of inorganic content (f_{ino}) is determined by TGA; ^{b)} The glass transition temperature (T_g) is determined by DSC; ^{c)} The glass transition temperature (T_g) is determined by DMA; ^{d)} The tensile strength and elongation at break are determined by the tensile tester; ^{e)} The elastic storage modulus (G') and the tan delta $(tan \delta)$ are determined by DMA.

www.afm-journal.de

16163028, 2024, 26, Downloaded from https://advan

witey.com/doi/10.1002/adfm.202315741 by Carnegie Mellon University. Wiley Online Library on [30.01/2025]. See the Terms and Conditions (https://onlinelibrary.wiley.com/terms-and-conditions) on Wiley Online Library for rules of use; OA acries are governed by the applicable Creative Commons

nanocomposites were investigated over a broad temperature range from -80 to 80 °C. Figure 3c,d presents the storage mechanical modulus G' and loss factor tan δ obtained from DMA for each M/SiO₂ and M/PB nanocomposite as a function of temperature. With the introduction of nanofillers, an increased G'value resulting from the filler-matrix interaction was expected. The *G'* values at 60 °C of each specimen are shown in Figure 3c inset and summarized in Table 1. Compared to the filler-free reference (G' = 1.81 MPa), M/SiO_{2,15} and M/SiO_{2,120} exhibited significant enhancements with 30 wt% SiO_2 loading (G' =4.00/2.99 MPa), where the higher value of M/SiO_{2.15} is associated with the larger surface area of the small size nanofillers. Moreover, further enhancements of G' values were observed for the M/SiO2 system to M/PB nanocomposites, as M/SiO215 (4.00 MPa) to M/PB₁₅-S (8.02 MPa), M/PB₁₅-L (4.72 MPa), and M/SiO_{2.120} (2.99 MPa) to M/PB₁₂₀-L (4.12 MPa), which is attributed to the better dispersion of the filler as well as the strong chemical/physical interaction between the SiO2 nanoparticles and the grafted PI ligands. Figure 3d shows the plots of the tan δ for the M/SiO₂ and M/PB samples, which illustrate the molecular motion of the polymer chains, the filler-matrix interaction among the rubber network as well as the viscoelasticity/rolling resistance of the nanocomposites. A stronger filler-matrix interaction leads to a lower tan $\delta_{\rm max}$ value. Besides the physical adsorption to the nanoparticle surfaces, the stable covalent bonding between the PI ligands and SiO₂ efficiently enhanced the filler-matrix interactions, as lower tan $\delta_{\rm max}$ values were observed in M/PB than in M/SiO $_2$ samples. On the other hand, tan δ values at 60 °C represent the rolling resistance property of the nanocomposites, relying on the friction among the filler-filler, filler-matrix, and matrix-matrix, which is strongly associated with the energy-saving efficiency in tire applications. [12,77,78] With the same size fillers, M/PB exhibits lower tan δ values and betterrolling resistance properties than M/SiO2 samples, which can be attributed to the superior dispersibility in the particle brush system.

Computational studies were conducted to further explore the reinforcing effect of the incorporation of SiO₂-g-PI particle brush in elastomer nanocomposites. Molecular Dynamic simulations were conducted to further explore the reinforcing effect of the incorporation of SiO₂-g-PI particle brush in elastomer nanocomposites. Using Kremer-Grest model to build a molecular model that is close to the experimental model, calculated glass transition temperature (T_o) based on free-volume theory, and measured mechanical properties based on the uniaxial tensile method. The simulated glass transition temperature (T_a) of M/PB nanocomposites is shown in Figure S11 (Supporting Information), which is obtained by identifying the temperature at which the specific volume density variates. The results of $T_{\rm g}$ confirm the accuracy of the simulation method. Qualitatively, the simulated trend in T_{σ} aligns with experimental observations, Figure 4d and Figure S9 (Supporting Information). There is a slight increase in T_g with an increase in graft chain length, and as the number of grafts increases, $T_{\rm g}$ begins to decrease. The entanglement effect induced by longer graft chains effectively constrains the movement of the matrix chains, increasing $T_{\rm g}$. Conversely, the M/PB₁₂₀-L possesses a higher number of grafting points and exhibits more pronounced interactions between graft chains. Snapshot images (Figures 4a-c and 5c) reveal a greater presence of cir-

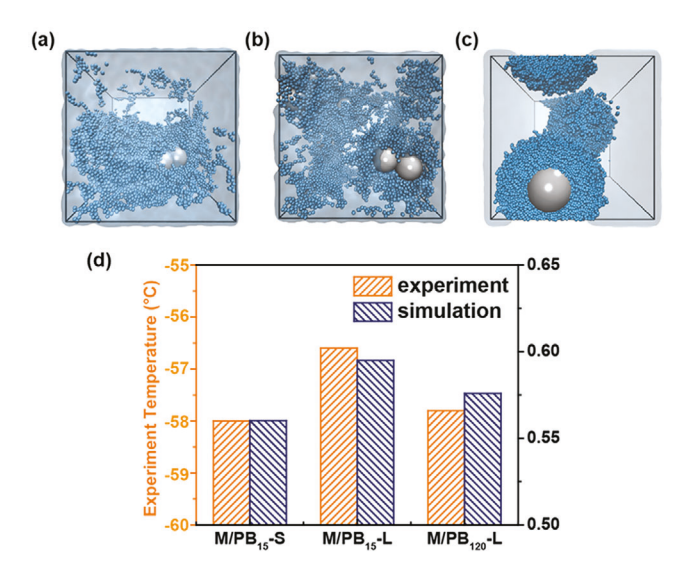


Figure 4. The snapshot of a) M/PB₁₅-L; b) M/PB₁₅-S; c) M/PB₁₂₀-L, gray spheres: the SiO2 nanoparticles, blue spheres: the PI chain beads; d) the comparison of glass transition temperatures (T_g) between simulation results and experimental results.

cular nanoparticles, indicating reduced hindrance to the movement of matrix chains, and consequently leading to a decrease

To verify and further investigate the mechanical performance of nanocomposites, stimulated uniaxial deformation tests of nanocomposites were carried out. The computational stressstrain curve for various systems is shown in Figure 5a. The mechanical performance of the three simulated systems is consistent with experimental results: the tensile modulus of the M/PB₁₂₀-L is prominently higher than M/PB₁₅-S and M/PB₁₅-L, with the modulus of M/PB₁₅-S being slightly higher than that of the M/PB₁₅-L. This indicates that increasing the number and chain length of grafted ligands has a positive impact on the mechanical performance of the system. Moreover, tuning the number of grafted chains is more efficient in improving the mechanical performance of the nanocomposites, as controlling the grafting density of the particle brushes is more applicable compared to achieving ultra-high molecular weight of the PI ligands.

With the increase in deformation, the entanglement point counts, denoted as $\langle Z \rangle$, in the M/PB₁₅-S and M/PB₁₅-L exhibit a roughly linear growth trend. In the case of M/SiO_{2 15/120} systems, the stretching process compels the molecular chains to move in the direction of the stretch. These moving molecular chains are more prone to creating new entanglement points, which is reflected in the simulations as an increase in the $\langle Z \rangle$ value with the progression of stretching. However, the system with shorter graft chains, M/PB₁₅-S, shows a slower rate of entanglement point growth compared to M/PB₁₅-L, which has longer graft chains, although both exhibit similar <Z> values in the low strain range (<0.25). This might be attributed to the fact that longer graft chains have a greater opportunity to form new entanglement points with the matrix chains during stretching, whereas shorter chains tend to quickly straighten under stress and cannot readily form new entanglement points.

16163028, 2024, 26, Downloaded

wiley.com/doi/10.1002/adfm.202315741 by Carnegie Mellon University, Wiley Online Library on [30/01/2025]. See the Terms

ns) on Wiley Online Library for rules of use; OA articles are governed by the applicable Creative Commons

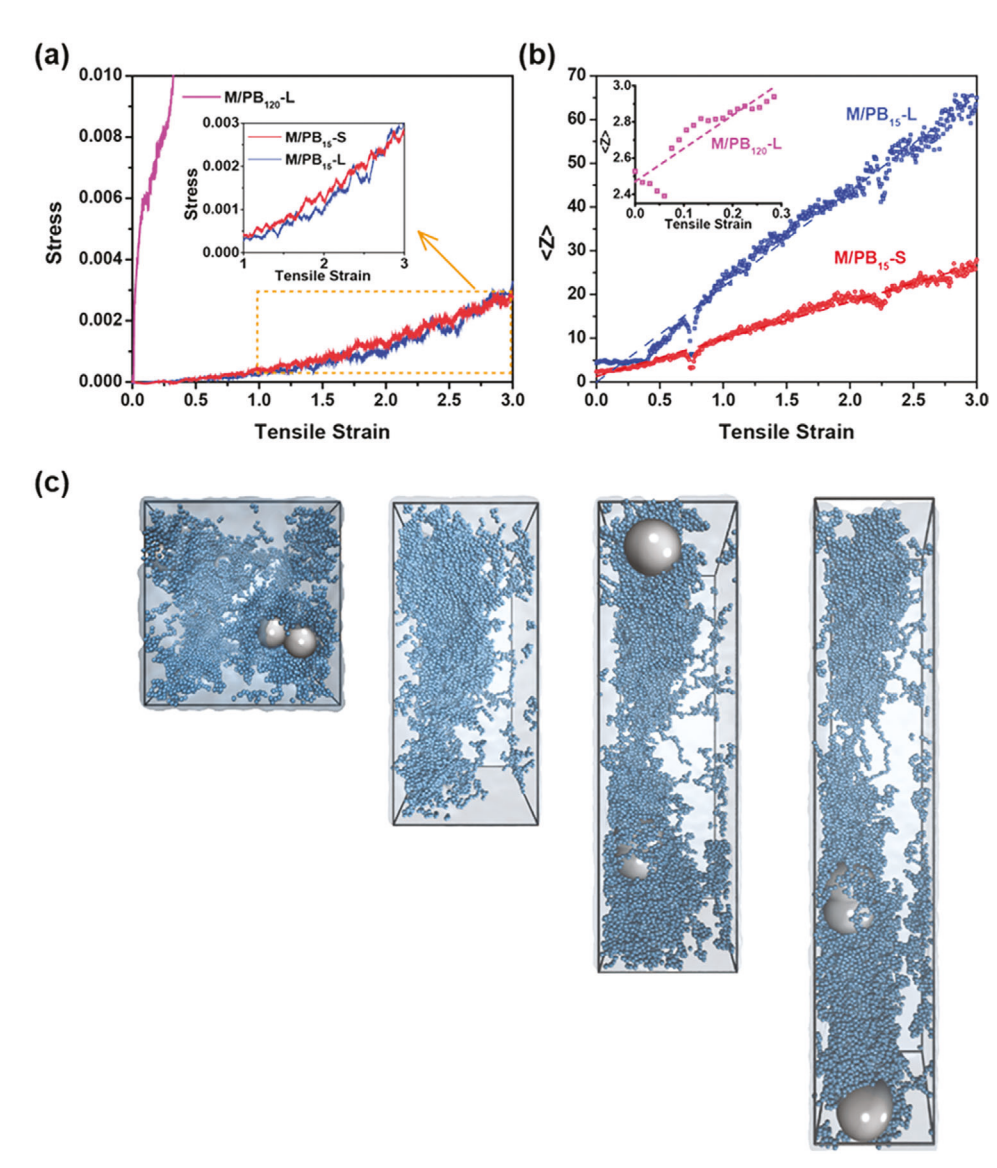


Figure 5. a) Stress–strain curves of three different systems from computational results; b) the average number of entanglements per chain, denoted by < Z >, versus tensile strain with different tensile strains; c) the snapshot of uniaxial deformation progress of M/PB₁₅-L, gray spheres: the SiO₂ nanoparticles, blue spheres: the PI chain beads.

3. Conclusion

High molecular weight linear PI and SiO_2 -g-PI particle brushes with different chain lengths and SiO_2 particle sizes were synthesized using ARGET ATRP. The M/PB have characteristic dynamical and structural features distinguished from both M/SiO₂ blends and bulk PI polymers, as a significant portion of polymers in M/PB nanocomposites became interfacial polymers, which influenced the interactions between filler-matrix, nanofiller microstructures as well as the macroscopic properties of the nanocomposites. The grafted PI ligands with tunable molar mass and grafting density promoted the filler-matrix interaction and facilitated the dispersion of SiO_2 in the nanocomposites. This resulted in remarkable mechanical properties improvement from M/SiO_{2,15} ($\sigma = 1.8$ MPa, $\varepsilon = 285\%$) to M/PB₁₅-S and M/PB₁₅-L ($\sigma = 5.0/5.8$ MPa, $\varepsilon = 510/680\%$). Furthermore, the

value of tan δ of M/PB₁₅-S, M/PB₁₅-L, and M/PB₁₂₀-L at 60 °C (0.116/0.119/0.056) experienced a noteworthy reduction compared to M/SiO_{2,15} and M/SiO_{2,120} (0.124/0.107), which indicated the rolling resistance is effectively reduced. This accomplishment has a potential promising impact on the commercial manufacturing of high-performance rubbers in tire applications.

4. Experimental Section

Materials in Brief: Monomer: isoprene (I, 99%, Alfa), Methyl methacrylate (MMA, 99%, Aldrich), Tris (2-dimethylaminoethyl)amine (Me₆TREN, 99%, Aladdin), tetrahydrofuran (THF, 99%, VWR), anisole (99%, Aladdin), ethyl 2-bromoisobutyrate (EBiB, 98%, Aladdin), methanol (99%, VWR), hexane (99%, VWR), acetone (99%, VWR), N,N-dimethylformamide (DMF, ≥99.8%, Aladdin), copper(II) bromide (CuBr₂, 99%, Aldrich), tin(II) 2-ethylhexanoate (Sn(EH)₂, 95%, Aldrich), 37% hydrofluoric

16163028, 2024, 26, Downloaded from https://advanced.

onlinelibrary wiley.com/doi/10.1002/adfin.202315741 by Carnegie Mellon University, Wiley Online Library on [30/01/2025]. See the Terms and Conditions (https://onlinelibrary.wiley.com/

nditions) on Wiley Online Library for rules of use; OA articles are governed by the applicable Creative Commons I

ADVANCED FUNCTIONAL MATERIALS

acid aqueous solution (HF, >99.99%, Aldrich), ammonium hydroxide aqueous solution (NH₄OH, 28.0-30.0%, TCI), dicumyl peroxide (DCP, 98%, Sigma–Aldrich), octadecyl 3-(3,5-di-*tert*-butyl-4-hydroxyphenyl) propionate (Irganox 1076, 98%, Aladdin). Silica nanoparticles, 30 wt% solutions in methyl isobutyl ketone (MIBK-ST) and isopropanol (IPA-ST-ZL), with effective diameter $d \approx 15.8$ nm and $d \approx 117.2$ nm, were kindly donated by Nissan Chemical Corp. and used as received.

Procedures for the Synthesis of Linear Polyisoprene(PI) by ARGET ATRP: Initiator (EBiB), solvents (anisole, DMF), CuBr $_2$, and Me $_6$ TREN were mixed thoroughly in a sealed thick-wall pressure bottle with a rubber plug. A stock solution of Sn(EH) $_2$ in anisole and purified isoprene in a round flask were prepared, separately. Both mixtures and the isoprene monomers were degassed by nitrogen purging, then the isoprene monomer and the Sn(EH) $_2$ solution were added into the pressure bottle to activate the catalyst complex, and the tube was immediately sealed and put into an oil bath set at the desired temperature. The reaction mixture was cooled to room temperature and added to cold methanol to precipitate the product. The molecular weight of the polymer was measured by SFC

Procedures for the Synthesis of SiO $_2$ -g-PI Particle Brushes by ARGET ATRP: Macro-initiator (SiO $_2$,15-Br/SiO $_2$,120-Br nanoparticles), solvents (anisole, DMF), CuBr $_2$, and Me $_6$ TREN were mixed thoroughly in a sealed thick-wall pressure bottle with a rubber plug. A stock solution of Sn(EH) $_2$ in anisole and purified isoprene in a round flask were prepared, separately. Both mixtures and the isoprene monomers were degassed by nitrogen purging, then the isoprene monomer and the Sn(EH) $_2$ solution were added into the pressure bottle to activate the catalyst complex, and the tube was immediately sealed and put into an oil bath set at the desired temperature. The reaction mixture was cooled to room temperature and added to cold methanol to precipitate the product. The molecular weight of the polymer was measured by SEC.

Procedures for Fabrication of SiO_2 -g-PI Particle Brushes/Linear PI Blends and SiO_2 Nanoparticles/Linear PI Blends: For each nanocomposite, SiO_2 -g-PI (PB₁₅-S, PB₁₅-L, PB₁₂₀-L) was dissolved in 200 mL of THF, and the appropriate amount of linear homopolymer PI matrix (L-1) was dissolved in THF to form a homogeneous solution. An antioxidant (Irganox 1076) was added at 0.5 wt% of PB/M mixtures to prevent degradation. These prepared solutions were stirred and sonicated for sufficient time until uniform mixtures were obtained at room temperature. Then 2 phr DCP was added as the coupling agent. THF in the system was removed during the stirring process at room temperature. The composites were cured at 151 °C.

Characterization—Size Exclusion Chromatography (SEC): Number-average molecular weights $(M_{\rm n})$ and molecular weight distributions $(M_{\rm w}/M_{\rm n})$ were determined by SEC. The SEC was conducted with a Waters 1515 pump and a Waters 2414 refractive index detector.

Characterization—Nuclear Magnetic Resonance (NMR): Polymerization was monitored by $^1\mathrm{H}$ NMR with a Bruker Advance 500 MHz NMR spectroscopy in CDCl $_3$ solvent.

Characterization—Scanning Electron Microscopy (SEM): The morphology of the samples and the distribution of the silica on the samples were examined by a S-4800 field emission scanning electron microscope (Hitachi Co., Japan) at an accelerating voltage of 5 kV.

Characterization—Atomic Force Microscopy (AFM): Bruker Multi-mode8 AFM was used to quantitatively characterize the nanoscale structure of SiO₂-g-PI/matrix and bare silica/matrix samples.

Characterization—Transmission Electron Microscopy (TEM): TEM was carried out using a Tecnai G2 F30 electron microscope operated at an acceleration voltage of 300 kV to characterize the morphology and distribution of silica of the cured composite samples. Before characterization, an ultramicrotome (Leica EMUC7) was used to make a nanosheet and a freshly cut surface at $-65\,^{\circ}\text{C}$.

Characterization—Thermogravimetric Analysis (TGA): TGA with STAR eSystem TGA2 (Mettler-Toledo International, Inc., Switzerland) was used to measure the fraction of SiO_2 in the SiO_2 -g-PI particle brushes.

Characterization—Differential Scanning Calorimetry (DSC): The glass transition temperature ($T_{\rm g}$) of linear PI homopolymers and SiO₂-g-PI particle brushes were measured by differential scanning calorimetry (DSC) with a DSC1 instrument (Mettler-Toledo International, Inc., Switzerland).

Characterization—Dynamic Mechanical Thermal Analysis (DMA): The dynamic mechanical properties were determined on a VA 3000 dynamic mechanical thermal analyzer (01 dB-Metravib Co., France) in the tension mode at a fixed frequency of 10 Hz.

Characterization—Mechanical Property Measurements: The static mechanical properties of the samples were obtained using a CMT4104 Electrical Tensile Tester (SANS) at a rate of 100 mm min⁻¹ at room temperature.

Characterization—Hardness Test: Shore A hardness was measured according to ASTM D2240 with a HPE II hardness apparatus (Bareiss Co, Germany).

Characterization—Small-Angle X-Ray Scattering (SAXS): Small-angle X-ray scattering measurements were done using a SAXS Xuess2-0 (Xenocs, France) with a Cu-K α source (0.154 nm wavelength and sample distance of 1682 mm).

Solid-State Nuclear Magnetic Resonance (NMR): The crosslinking density was measured by Bruker 400 WB AVANCE III NMR spectrometer (Bruker Corporation, Germany). The field intensity was 9.4T and the frequency range from 6 to 364 MHz.

Characterization—Abrasion Resistance Test: The abrasion resistance of the samples was tested by a rotating cylindrical drum device (Model TST-P307, TST Testing Instruments Co., LTD, China). The rotating speed of the drum is 40 ± 1 r min⁻¹, the grinding stroke is 40 m, and the sample load is 10+0.2 N.

Supporting Information

Supporting Information is available from the Wiley Online Library or from the author.

Acknowledgements

Y.L. and Z.W. contributed equally to this work. This work was supported by the National Key R&D Program of China (2022YFB3704700) and the National Science Foundation for Young Scientists of China (52003016). X.Q. gratefully acknowledges financial support from the China Scholarship Council. K.M. acknowledges support from NSF (DMR 2202747).

Conflict of Interest

The authors declare no conflict of interest.

Data Availability Statement

The data that support the findings of this study are available from the corresponding author upon reasonable request.

Keywords

atom transfer radical polymerization, elastic modulus, isoprene, particle brush, silica

Received: December 10, 2023 Revised: January 22, 2024 Published online: February 29, 2024

- [1] J. Njuguna, K. Pielichowski, Adv. Eng. Mater. 2003, 5, 769.
- [2] S. M. Oh, S. Y. Kim, ACS Appl. Mater. Interfaces 2023, 15, 4527.
- [3] H. Luo, S. Chen, L. Liu, X. Zhou, C. Ma, W. Liu, D. Zhang, ACS Sustainable Chem. Eng. 2019, 7, 3145.

16163028, 2024, 26, Downloaded wiley.com/doi/10.1002/adfm.202315741 by Carnegie Mellon University, Wiley Online Library on [30/01/2025]. See the Terms

) on Wiley Online Library for rules of use; OA articles are governed by the applicable Creative Commons

- [4] T. Kashiwagi, F. Du, J. F. Douglas, K. I. Winey, R. H. Harris, J. R. Shields, Nat. Mater. 2005, 4, 928.
- [5] A. K. Kota, B. H. Cipriano, M. K. Duesterberg, A. L. Gershon, D. Powell, S. R. Raghavan, H. A. Bruck, *Macromolecules* 2007, 40, 7400
- [6] R. Gangopadhyay, A. De, Chem. Mater. 2000, 12, 608.
- [7] A. C. Balazs, T. Emrick, T. P. Russell, Science 2006, 314, 1107.
- [8] S. Wu, M. Qiu, Z. Tang, B. Guo, J. Phys. Chem. C 2017, 121, 28594
- [9] C. Mary, D. Philippon, L. Lafarge, D. Laurent, F. Rondelez, S. Bair, P. Vergne, *Tribol. Lett.* 2013, 52, 357.
- [10] M. K. Dibbanti, M. Mauri, L. Mauri, G. Medaglia, R. Simonutti, J. Appl. Polym. Sci. 2015, 132, 42700.
- [11] D. Dhara, M. A. Rahman, Z. Abbas, E. Ruzicka, B. Benicewicz, S. K. Kumar, ACS Macro Lett. 2022, 11, 1325.
- [12] X. Qin, J. Wang, Y. Zhang, Z. Wang, S. Li, S. Zhao, T. Tan, J. Liu, L. Zhang, K. Matyjaszewski, Adv. Funct. Mater. 2020, 30, 2003429.
- [13] C. M. Hui, J. Pietrasik, M. Schmitt, C. Mahoney, J. Choi, M. R. Bockstaller, K. Matyjaszewski, Chem. Mater. 2014, 26, 745.
- [14] J. Jiao, X. Sun, T. J. Pinnavaia, Adv. Funct. Mater. 2008, 18, 1067.
- [15] M. Endo, T. Noguchi, M. Ito, K. Takeuchi, T. Hayashi, Y. A. Kim, T. Wanibuchi, H. Jinnai, M. Terrones, M. S. Dresselhaus, Adv. Funct. Mater. 2008, 18, 3403.
- [16] J. Fröhlich, W. Niedermeier, H. D. Luginsland, Composites, Part A 2005. 36, 449.
- [17] J. B. Hooper, K. S. Schweizer, Macromolecules 2006, 39, 5133.
- [18] G. Lindenblatt, W. Schärtl, T. Pakula, M. Schmidt, Macromolecules 2000, 33, 9340.
- [19] P. G. De Gennes, Macromolecules 1981, 14, 1637.
- [20] C. Bechinger, D. Rudhardt, P. Leiderer, R. Roth, S. Dietrich, Phys. Rev. Lett. 1999, 83, 3960.
- [21] G. P. Baeza, A.-C. Genix, C. Degrandcourt, L. Petitjean, J. Gummel, R. Schweins, M. Couty, J. Oberdisse, *Macromolecules* 2013, 46, 6621
- [22] G. P. Baeza, A.-C. Genix, C. Degrandcourt, L. Petitjean, J. Gummel, M. Couty, J. Oberdisse, *Macromolecules* 2013, 46, 317.
- [23] A. Bouty, L. Petitjean, J. Chatard, R. Matmour, C. Degrandcourt, R. Schweins, F. Meneau, P. Kwasńiewski, F. Boué, M. Couty, J. Jestin, Faraday Discuss. 2016, 186, 325.
- [24] A. Bouty, L. Petitjean, C. Degrandcourt, J. Gummel, P. Kwaśniewski, F. Meneau, F. Boué, M. Couty, J. Jestin, *Macromolecules* 2014, 47, 5365
- [25] M. Bonnevide, A. M. Jimenez, D. Dhara, T. N. T. Phan, N. Malicki, Z. M. Abbas, B. Benicewicz, S. K. Kumar, M. Couty, D. Gigmes, J. Jestin, *Macromolecules* 2019, 52, 7638.
- [26] P. Akcora, H. Liu, S. K. Kumar, J. Moll, Y. Li, B. C. Benicewicz, L. S. Schadler, D. Acehan, A. Z. Panagiotopoulos, V. Pryamitsyn, V. Ganesan, J. Ilavsky, P. Thiyagarajan, R. H. Colby, J. F. Douglas, Nat. Mater. 2009, 8, 354.
- [27] C. Chevigny, F. Dalmas, E. Di Cola, D. Gigmes, D. Bertin, F. Boué, J. Jestin, Macromolecules 2011, 44, 122.
- [28] S. Srivastava, P. Agarwal, L. A. Archer, Langmuir 2012, 28, 6276.
- [29] Z. M. Abbas, M. Tawfilas, M. M. Khani, K. Golian, Z. M. Marsh, M. Jhalaria, R. Simonutti, M. Stefik, S. K. Kumar, B. C. Benicewicz, *Polymer* 2019, 171, 96.
- [30] S. Granick, H. Hu, Langmuir 1994, 10, 3857.
- [31] D. Kleshchanok, P. R. Lang, Langmuir 2007, 23, 4332.
- [32] J. B. Hooper, K. S. Schweizer, Macromolecules 2005, 38, 8858.
- [33] Y. Wei, Y. Xu, A. Faraone, M. J. A. Hore, ACS Macro Lett. 2018, 7, 699.
- [34] Y. Wei, Q. Chen, H. Zhao, P. Duan, L. Zhang, J. Liu, *Langmuir* 2023, 39, 11003.
- [35] K. Matyjaszewski, H. Dong, W. Jakubowski, J. Pietrasik, A. Kusumo, Langmuir 2007, 23, 4528.

- [36] K. Matyjaszewski, W. Jakubowski, K. Min, W. Tang, J. Huang, W. A. Braunecker, N. V. Tsarevsky, Proc. Natl. Acad. Sci. U. S. A. 2006, 103, 15200
- [37] W. Jakubowski, K. Matyjaszewski, Angew. Chem. 2006, 118, 4594.
- [38] W. Jakubowski, K. Min, K. Matyjaszewski, Macromolecules 2005, 39, 39.
- [39] N. Corrigan, K. Jung, G. Moad, C. J. Hawker, K. Matyjaszewski, C. Boyer, Prog. Polym. Sci. 2020, 111, 101311.
- [40] C. Boyer, N. A. Corrigan, K. Jung, D. Nguyen, T.-K. Nguyen, N. N. M. Adnan, S. Oliver, S. Shanmugam, J. Yeow, Chem. Rev. 2016, 116, 1803.
- [41] M. Schöps, H. Leist, A. DuChesne, U. Wiesner, Macromolecules 1999, 32, 2806.
- [42] H. S. Yu, J. S. Kim, V. Vasu, C. P. Simpson, A. D. Asandei, ACS Catal. 2020. 10. 6645.
- [43] W. A. Braunecker, K. Matyjaszewski, Prog. Polym. Sci. 2007, 32, 93.
- [44] X. Pan, M. Fantin, F. Yuan, K. Matyjaszewski, Chem. Soc. Rev. 2018, 47, 5457.
- [45] F. Lorandi, K. Matyjaszewski, Isr. J. Chem. 2020, 60, 108.
- [46] F. di Lena, K. Matyjaszewski, Prog. Polym. Sci. 2010, 35, 959.
- [47] K. Matyjaszewski, Macromolecules 2012, 45, 4015.
- [48] K. Matyjaszewski, N. V. Tsarevsky, J. Am. Chem. Soc. 2014, 136, 6513.
- [49] K. Matyjaszewski, N. V. Tsarevsky, Nat. Chem. 2009, 1, 276.
- [50] N. V. Tsarevsky, K. Matyjaszewski, Chem. Rev. 2007, 107, 2270.
- [51] K. Matyjaszewski, Adv. Mater. 2018, 30, 1706441.
- [52] K. Matyjaszewski, J. Xia, Chem. Rev. 2001, 101, 2921.
- [53] J. Wang, K. Matyjaszewski, J. Am. Chem. Soc. 1995, 117, 5614.
- [54] D. Benoit, E. Harth, P. Fox, R. M. Waymouth, C. J. Hawker, Macromolecules 2000, 33, 363.
- [55] S. Harrisson, P. Couvreur, J. Nicolas, Macromolecules 2011, 44,
- [56] V. Jitchum, S. Perrier, Macromolecules 2007, 40, 1408.
- [57] S. Harrisson, J. Nicolas, A. Maksimenko, D. T. Bui, J. Mougin, P. Couvreur, Angew. Chem., Int. Ed. 2013, 52, 1678.
- [58] F. Lauterbach, M. Rubens, V. Abetz, T. Junkers, Angew. Chem., Int. Ed. 2018, 57, 14260.
- [59] M. Kamigaito, T. Ando, M. Sawamoto, Chem. Rev. 2001, 101, 3689.
- [60] C. J. Hawker, A. W. Bosman, E. Harth, Chem. Rev. 2001, 101, 3661.
- [61] Z. Wang, J. Lee, Z. Wang, Y. Zhao, J. Yan, Y. Lin, S. Li, T. Liu, M. Olszewski, J. Pietrasik, M. R. Bockstaller, K. Matyjaszewski, ACS Macro Lett. 2020, 9, 806.
- [62] R. Yin, Z. Wang, M. R. Bockstaller, K. Matyjaszewski, Polym. Chem. 2021, 12, 6071.
- [63] J. Yan, M. R. Bockstaller, K. Matyjaszewski, Prog. Polym. Sci. 2019, 100, 101180.
- [64] J. Shen, J. Liu, Y. Gao, D. Cao, L. Zhang, Langmuir 2011, 27, 15213.
- [65] Q. Chen, S. Gong, J. Moll, D. Zhao, S. K. Kumar, R. H. Colby, ACS Macro Lett. 2015, 4, 398.
- [66] A. Mujtaba, M. Keller, S. Ilisch, H. J. Radusch, T. Thurn-Albrecht, K. Saalwächter, M. Beiner, Macromolecules 2012, 45, 6504.
- [67] E. Wisse, A. J. H. Spiering, F. Pfeifer, G. Portale, H. W. Siesler, E. W. Meijer, Macromolecules 2009, 42, 524.
- [68] Z. Wang, J. Liu, S. Wu, W. Wang, L. Zhang, Phys. Chem. Chem. Phys. 2010, 12, 3014.
- [69] E. Senses, P. Akcora, Macromolecules 2013, 46, 1868.
- [70] A. Mujtaba, M. Keller, S. Ilisch, H. J. Radusch, M. Beiner, T. Thurn-Albrecht, K. Saalwächter, ACS Macro Lett. 2014, 3, 481.
- [71] S. Cheng, A. P. Holt, H. Wang, F. Fan, V. Bocharova, H. Martin, T. Etampawala, B. T. White, T. Saito, N.-G. Kang, M. D. Dadmun, J. W. Mays, A. P. Sokolov, *Phys. Rev. Lett.* 2016, 116, 038302.
- [72] B. Carroll, S. Cheng, A. P. Sokolov, Macromolecules 2017, 50, 6149.



www.advancedsciencenews.com



www.afm-journal.de

16163028, 2024, 26, Downloaded

online library.wiley.com/doi/10.1002/adfm.202315741 by Carnegie Mellon University, Wiley Online Library on [30/01/2025]. See the Terms and Conditions (https://onlinelibrary.wiley

and-conditions) on Wiley Online Library for rules of use; OA articles are governed by the applicable Creative Commons License

- [73] I. Popov, B. Carroll, V. Bocharova, A.-C. Genix, S. Cheng, A. Khamzin, A. Kisliuk, A. P. Sokolov, *Macromolecules* 2020, 53, 4126.
- [74] N. Jouault, J. F. Moll, D. Meng, K. Windsor, S. Ramcharan, C. Kearney, S. K. Kumar, ACS Macro Lett. 2013, 2, 371.
- [75] D. Zhao, S. Ge, E. Senses, P. Akcora, J. Jestin, S. K. Kumar, *Macro-molecules* 2015, 48, 5433.
- [76] X. Qin, B. Han, J. Lu, Z. Wang, Z. Sun, D. Wang, T. P. Russell, L. Zhang, J. Liu, Nano Energy 2018, 48, 180.
- [77] J. Liu, Z. Zheng, F. Li, W. Lei, Y. Gao, Y. Wu, L. Zhang, Z. L. Wang, Nano Energy 2016, 28, 87.
- [78] J. Wang, M. Wang, X. Zhang, Y. Han, Y. Wu, D. Wang, X. Qin, Y. Lu, L. Zhang, ACS Appl. Mater. Interfaces 2023, 15, 45388.